SSRG International Journal of Electrical and Electronics Engineering
ISSN: 2348-8379/ https://doi.org/10.14445/23488379/IJEEE-V11I8P127

Volume 11 Issue 8, 309-322, August 2024

Original Article

Analysis of Solar PV Array Integration with DC-DC Converter and Battery-Integrated UPQC for Microgrid Power Quality Enhancement

R. Suja[1], K. Murugesan[2], R.Vignesh[3], Manjunatha[4]

[1]*Faculty of Electrical Engineering, Rajas Institute of Technology, Tamilnadu, India.*
[2]*Department of Electrical and Electronics Engineering, Sri Sivasubramaniya Nadar College of Engineering, Tamilnadu, India.*
[3]*Department of Biomedical Engineering, P.S.R. Engineering College, Tamilnadu, India.*
[4]*Department of Mechanical Engineering, New Horizon College of Engineering, Karnataka, India.*

[1]*Corresponding Author : sujapet1976@gmail.com*

Received: 12 June 2024 Revised: 16 July 2024 Accepted: 12 August 2024 Published: 31 August 2024

Abstract *- PV (Photovoltaic) fed UPQC (Unified Power Quality Conditioner) systems are innovative solutions for improving Power Quality (PQ) in microgrids that incorporate solar PV arrays. These systems combine the advantages of solar power generation with the power conditioning capabilities of UPQC technology to enhance the overall efficiency and reliability of microgrids. Super-Lift Luo Converter, which significantly contributes to optimizing the utilization of solar power and improving the power quality of the microgrid, is implemented in this work. By integrating the converter into UPQC, the PV system actively compensates for PQ issues in the microgrid. The Type-2 Fuzzy Logic Controller (T2 FLC) based MPPT (Maximum Power Point Tracking) control mechanism helps regulate the output voltage and assures a constant and high-quality power supply to the loads. Additionally, battery storage allows for the capture and storage of excess energy generated by PV arrays during periods of high solar irradiation. This stored energy is used in periods of low solar generation or high load demand, effectively balancing the energy supply and demand. Furthermore, the current harmonics are eliminated using the PI controller-assisted DQ theory. The entire proposed system is verified using the MATLAB platform.*

Keywords *- PV system, UPQC, Super-Lift Luo converter, microgrid, T2 FLC-based MPPT.*

1. Introduction

The emergence of microgrid systems signifies a pivotal shift in power distribution paradigms. These innovative networks leverage a diverse array of technologies and strategies to enhance energy resilience, efficiency, and sustainability. By seamlessly integrating distributed generators, renewable energy sources, energy storage solutions, and advanced control algorithms, microgrids offer a robust platform for addressing the evolving needs of modern society. [1].

The handling of power flow among the AC to the DC grid and the mitigation of power quality concerns are two major tasks that need to be performed during the implementation of the power distribution grid and microgrid [3, 2]. In microgrids, Power Quality (PQ) issues are broadly classified into utility-related challenges and consumer-related issues.

Consumer-related problems include Total Harmonic Distortion (THD), unbalanced loads, reactive power demand, and delayed power factor. Utility-related concerns involve voltage sag/swell, flicker, notches, unbalanced sources, and interruptions. The most substantial PQ distortions arise on the side of utility as voltage loss and on the consumer side as distortion caused by harmonics. Such PQ distortions degrade the effectiveness of the power system connection and degrade the lifespan of the corresponding devices [5].

Recent studies indicate that Point of Common Coupling (PCC) uses the inexpensive tailored power device known as the UPQC to guard against PQ distortion for both the utility and the customer. Currently, many researchers are focusing on merging both storage and renewable energy, as well as custom power devices, to address the criteria of increased PQ, renewable energy generation, and continuous power supply for essential loads. When functioning in stand-alone mode, battery energy storage is crucial for green energy systems [6].

The battery's higher cost becomes acceptable when the system is utilized for essential uses, which include healthcare facilities, electronics industries, and so on when a constant supply of high-quality power is required.

DC-DC converters serve diverse purposes within power electronics applications. Boost converters are commonly used in PV applications for converting voltage; however, a step-up voltage ratio is only achievable [8, 9]. Buck-Boost [10, 11] converters are used to operate MPPT, although they face higher transitioning stress and poor voltage conversion efficiency. Furthermore, buck-boost converters necessitate huge input capacitors, and their discontinuous input current limits their capacity to conduct optimum MPPT in their lack of big decoupling capacitors.

The Cuk [12], SEPIC [13, 14], and Luo [15] converters are now available to solve the drawbacks of buck-boost converters. These converters have low switching losses, excellent efficiency, and voltage moderation, allowing for adaptable operation. However, these converters lack the ability to adjust voltage levels rapidly. Henceforth, this research suggests a Super-Lift Luo converter to overcome the aforementioned limitations. In addition, this converter further improves the system efficiency with reduced ripple content.

The UPQC operates as a series-shunt converter with a shared DC link capacitor. Precise DC link voltage control is vital for enhancing the compensating capability. Unlike traditional UPQC devices, which rely on PI controllers for DC link voltage regulation, achieving optimal control of DC link voltage is essential for maximizing compensating capacity [16]. Yet, conventional PI controllers require linear mathematical equations, which cannot effectively regulate DC link voltage during high voltage loss and dynamic operating conditions. Currently, many scientists have proposed several MPPT algorithms for obtaining the utmost power from solar panels with stabilized DC link voltage. As addresses to the drawbacks of the aforesaid procedures, the Perturbation and Observation Incremental Conductance approaches are proposed [17-19]. This algorithm represents the best way to identify the ideal power-point.

Nonetheless, these approaches have minimal size fluctuation while the climate condition changes often. In [20, 21], FLC is considered one of the greatest effective manners for managing system unpredictability and non-linear behavior. The FLC is extremely useful for dealing with PV's unexpected and randomized nature, which has been mimicked in the dynamic behaviors of PV. However, this method is less accurate in tracking the maximum power from the PV system. Thus, these limitations are tackled by using a T2 FLC-based MPPT controller. It effectively enhances the converter's DC link voltage and conversion efficiency.

In [22], the SVPWM technique is used to improve the compensation capability of the UPQC system. However, SVPWM is not a suitable technique in terms of handling harmonic content. Moreover, its sensitivity to noise and errors affects the output waveform stability and quality. In [23], an optimized FOPID controller is implemented for UPQC control, but this technique grapples with its heightened sensitivity to parameter tuning. PI controller-based UPQC control implemented in [24] struggles with limitations in transient conditions in spite of providing quick power balance.

This work identifies a significant research gap in improving converter performance and PQ management in microgrid systems. Conventional UPQC control approaches often falter in dynamic conditions and high-voltage loss scenarios. The P&O and IC MPPT algorithms, while effective under stable conditions, struggle with fluctuations caused by varying climatic conditions. Furthermore, the FLC offers improved management of system unpredictability and non-linear behavior but lacks the precision needed for optimal power tracking in PV systems.

To address these gaps, this work suggests the implementation of a Super-Lift Luo converter, which aims to overcome the limitations of existing converters by enhancing system efficiency and reducing ripple content. Additionally, this work explores the novel application of T2 FLC-based MPPT controllers to improve DC link voltage stability and conversion efficiency. This approach promises to significantly advance the performance and reliability of microgrid systems, offering a more effective solution to the challenges of PQ and energy management.

2. Proposed System Description

In this research, a PV-powered UPQC layout, as shown in Figure 1, is established with the intention of reducing such PQ problems and encouraging the production of green energy. The DC link voltage stays at the appropriate intended value using an efficient control system.

The produced output from PV is improved with fewer switching losses with the adoption of a Super-Lift Luo converter. The T2 FLC-based MPPT receives the output of the PV system current and voltage as input, and it delivers the necessary variation in the duty cycle command. The resulting signal is received by the PWM generator, which controls the operation of the converter by producing pulses. The converter's regulated output, which has the expected voltage level, is sent to the DC link.

The series and shunt converters of UPQC are regulated using PI controller-assisted d-q theory. Here, the series converter reduces the load side harmonic, sag, and swell concerns at the PCC. The shunt converter regulates the DC capacitor voltage, supplying both voltage source converters and eliminating reactive and harmonic currents on the source side. D-Q theory is employed to generate reference current signals. Pulses produced from the PWM generator regulate the functioning of series and shunt compensators in accordance with reference current and regulation signal from the PI controller. Henceforth, the PQ problems are mitigated with high precision.

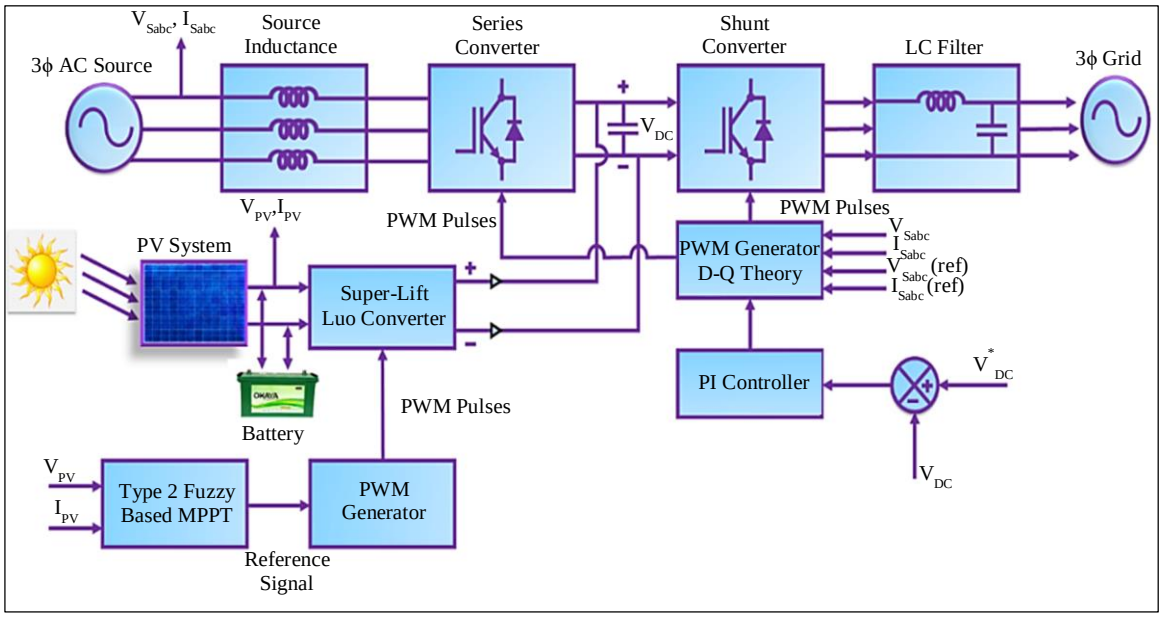

Fig. 1 Schematic representation of the proposed PV-fed UPQC model

3. Proposed Modelling

3.1. Modelling of UPQC

The UPQC enhances power quality in electrical networks by addressing issues like current harmonics, reactive power, voltage regulation, and interruptions. It includes shunt and series compensators: shunt for voltage fluctuations and series for current disruptions.

Basic Phasor Operation: The UPQC is represented by an ideal current source and an ideal voltage source in its essential specification. The reference voltage for the UPQC (V_s) is obtained from

$$V_{in}\angle\theta = V_{pen}\angle\beta + V_{ph}\angle\delta \quad (1)$$

Where V_{pen} the UPQC's penetration voltage and V_{ph} is the load voltage. Determining the amplitude and constant phase angles of V_{pen} is essential for stabilizing the load voltage at its maximum rating during a power factor-provided load and voltage sag. However, there exist infinite possibilities for V_{pen}. To optimize the loading of UPQC, the unique control approach proposed in this paper recalculated this injection angle. The expression for load current from the source is

$$\mathrm{I_{ph}}\angle\delta - \theta = \mathrm{I_{in}}\angle\theta + \mathrm{I_c}\angle\delta \quad (2)$$

This indicates the angle at which the load current (I_{ph}) lags behind the peak current (V_{ph}). Since the power supply is considered to be the primary active element of load current, $\delta = 0$. The supply voltage is initially enough in Stage 1:

$$\mathrm{V_{in}} = \mathrm{V_{ph1}} = \mathrm{V_{in1}} = \mathrm{Constant} = \mathrm{V_0} \quad (3)$$

Accordingly, the current is provided by IC_1, when angle β = +90; it is assumed that the power factor lags the voltage phase angle in power systems.

In Stage 2, the electrical supply voltage magnitude has dropped to V_{in2}, necessitating action from the UPQC to raise V_{ph2} back to its previous magnitude ($|V_{ph1}| = |V_{ph2}|$). This is accomplished by the injection of series voltage V_{inj} and selecting the load voltage between 0 and 90°, along with the appropriate magnitude of V_{inj}.

$$\mathrm{I_{in2}}\cos\beta = \mathrm{I_{ph2}}\cos\theta \quad (4)$$

$$\mathrm{I_{c2}} = \frac{\mathrm{I_{ph2}}\sin(\theta-\beta)}{\cos\beta} \quad (5)$$

Both active filters infuse reactive power into the load if $\alpha < \phi$. It's significant to note that this drooping voltage is such that, for a certain load power factor, angle equals, and from Equation (4) it is able to be deduced that $I_{S2} = I_{L1}$. It is assumed that the load current is stable.

$$\mathrm{I_{L1}} = \mathrm{I_{L2}} = \mathrm{I_0} \quad (6)$$

In a basic lagged power factor of $cos\phi$. The load maintains a constant demand for active power, which is balanced by the performance of the power source.

$$\mathrm{V_s I_s} = \mathrm{V_L I_L}\cos\emptyset = \mathrm{Constant} \quad (7)$$

Sag occurs whenever $|\mathrm{V_{s2}}|<|\mathrm{V_{s1}}|$ and per-unit voltage sag is indicated as x.

$$\mathrm{V_{s2}} = (1-\mathrm{x})\mathrm{V_{s1}} = (1-\mathrm{x})\mathrm{V_0} \quad (8)$$

To maintain a constant active power during a voltage sag, $V_{s1}, I_{s1} = V_{s2}, I_{s2}$ and,

$$I_{s2} = \frac{V_0 I_L \cos\emptyset}{V_0(1-x)} = I_0 \frac{\cos\emptyset}{(1-x)} \quad (9)$$

Hence,

$$V_{L2}\sin \propto = V_{inj}\sin\gamma \quad (10)$$

$$V_{L2}\cos \propto = V_{s2} + V_{inj}\cos\gamma \quad (11)$$

From the Equations (5) to (10),

$$V_{inj}^2 = V_0^2 x^2 + 2V_0^2(1-x)(1-\cos \propto) \quad (12)$$

The following formula represents the series converter's apparent power:

$$|V_{inj}||I_{s2}| = V_o I_0 \cos\emptyset \frac{\sqrt{x^2+2(1-x)(1-\cos\propto)}}{1-x} \quad (13)$$

Which results,

$$I_{c2}\cos \propto = I_{L2} + V_{inj}\sin(\emptyset - \propto) \quad (14)$$

The perceived power rating consequently is modelled by,

$$I_{c2}V_{12} + I_{c2}^2 Z_{SLC} = I_{L2}\left(V_0 \frac{\sin(\emptyset-\propto)}{\cos\propto} + I_{L2}\left(\frac{\sin(\emptyset-\propto^2)}{\cos\propto}\right)Z_{SLC}\right) \quad (15)$$

Where ZSLC is the synchronous linked converter's impedance when (13) and (15) are added together, the overall apparent power consumption of UPQC is written as,

$$\begin{cases} VA - UPQC = V_{op}I_{op}(\theta, x, \beta) + G_2(\theta,\beta)) + I_{op}^2 G_2^2(\theta,\beta)Z_{SLC} \\ G_1(\theta, x, \beta) = \cos\theta \frac{\sqrt{x^2+2(1-x)(1-\cos\beta)}}{(1-x)} \\ G_2(\theta,\beta) = \frac{\sin(\emptyset-\beta)}{\cos\beta} \end{cases} \quad (16)$$

As a result, the VA loading relies on a forward angle of VL for a particular load power factor angle α and voltage sag x p.u. The minimal VA is reached when $\phi = \alpha$, resulting in $I_{S2} = I_{L2}$ *and* $I_{c2} = 0$. In these circumstances, the recommended injected voltage is provided by,

$$V_{inj} = V_{oj}\sqrt{x^2 + 2(1-x)(1-\cos\emptyset}} \quad (17)$$

Similarly, the voltage advance angle of the source current is provided by,

$$\sin\gamma = \frac{\sqrt{1-\cos^2\alpha}}{\sqrt{x^2}+2(1-x)(1-\cos\emptyset)} \quad (18)$$

Thus, (17) and (18) are control formulas that determine whether UPQC uses a proper control approach to achieve the optimal angle of voltage injection.

3.2. Modelling of PV System

Solar PV-based power plants are emerging as significant sources of clean energy due to their advantages over other forms of renewable power, including no fuel requirement, zero pollution, minimal upkeep, and reduced noise. The equivalent solar energy system circuitry schematic is depicted in Figure 2.

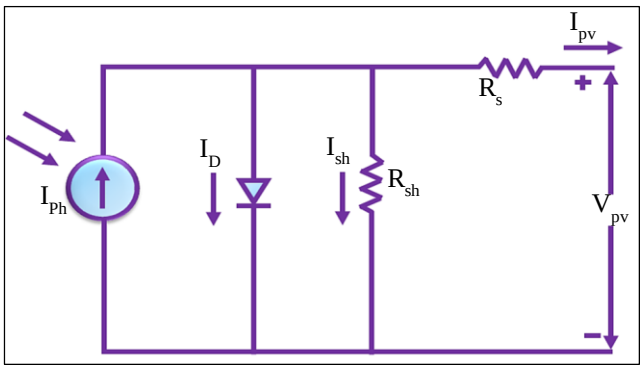

Fig. 2 Equivalent circuit representation of PV

Following is an equation connecting the PV panel's voltage and current.

$$V_{PV} = n_S \frac{AKT}{q} \ln\left\{\frac{n_p I_{SC} - I_{PV} + n_p I_o}{n_p I_o}\right\} - \frac{n_S}{n_p} I_{PV} R_S \quad (19)$$

$$P_{PV} = V_{PV} * I_{PV} \quad (20)$$

The PV system operates efficiently at MPP for each parameter. Figure 3 demonstrates the effectiveness of the PV array.

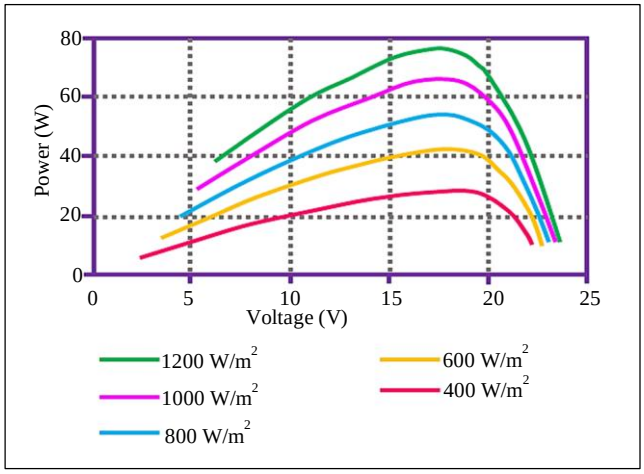

Fig. 3 PV system performance at $T = 25°C$

A Super-Lift Luo converter is chosen to attain the desired output voltage from PV, which is elaborated on in the subsequent section.

3.3. Modelling of Super-Lift Luo Converter

It is derived from the conventional Luo converter and features additional circuitry that enables it to achieve even higher voltage conversion ratios. Such converters are frequently employed in switch mode power supplies, manufacturing processes, and computer interface equipment, particularly for high-voltage applications. Figure 4 depicts the super lift Luo converter. It has the power switch ($IGBT$) S, the diodes $D_1 and\ D_2$, the capacitors $C_1 and\ C_2$, the inductor L, and the load resistance R. The working operation of the proposed converter operating in continuous conduction mode is illustrated in Figures 5(a) and (b). When switch S is in the ON position in Figure 5 (a), the voltage across the capacitor C_1 charges to V_{in}. With voltage V_{in}, the current i_L passing through the inductor L rises. In Figure 5 (b), the inductor current i_L drops with voltage ($V_o - 2\ V_{in}$) while switch S is in the off state. Consequently, the inductor's current i_L ripple is,

$$\Delta i_L = \frac{V_{in}}{L_i} dT = \frac{V_o - 2V_{in}}{L_I} dT \quad (21)$$

$$V_0 = \frac{2-d}{1-d} V_{in} \quad (22)$$

The obtained transfer gain of voltage is,

$$G = \frac{V_0}{V_{in}} = \frac{2-d}{1-d} \quad (23)$$

When the S is activated, the input current i_{in} is equal to (i_L+i_{C1}), and when turning off, it is just equal to i_L. The i_L and i_{C1} are the same during the switching-off of the capacitor. The average charge over the capacitor C_1 is supposed to stay constant in steady condition.

$$i_{in-off} = i_{L-off} = i_{C1-off} \quad (24)$$

$$i_{in-on} = i_{L-on} + i_{ci-on} \quad (25)$$

$$dTi_{c1-on} = (1-d)Ti_{c1-off} \quad (26)$$

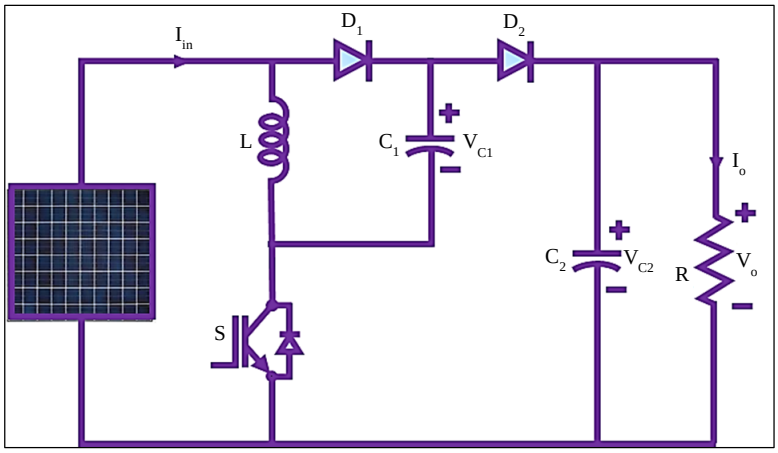

Fig. 4 Equivalent circuit of super lift luo converter

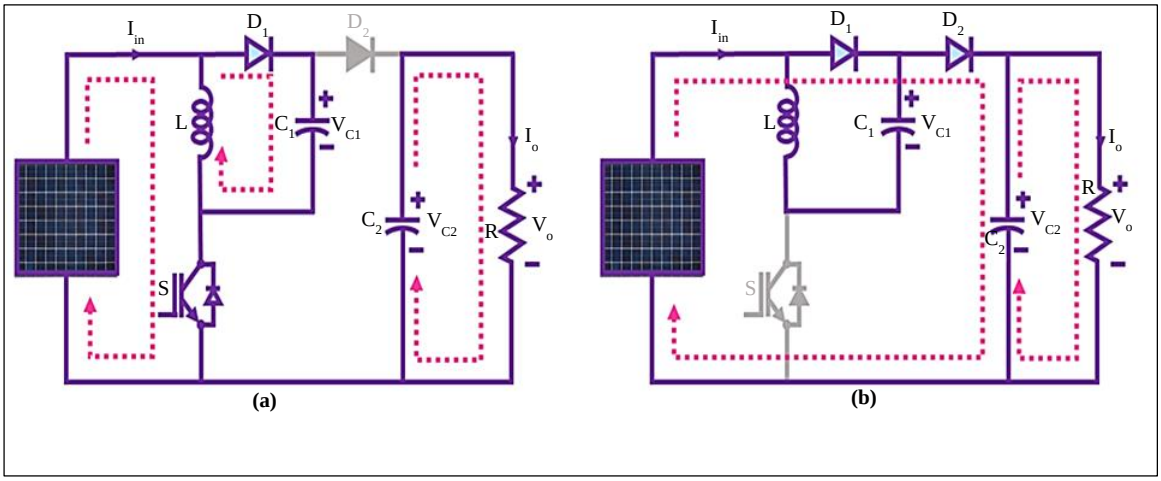

Fig. 5 (a) Stage 1, and (b) Stage 2.

The i_L is similar to its average current i_L if inductor L is sufficiently high. Thus,

$$i_{in-off} = i_{c1-off} = I_L \quad (27)$$

$$i_{in-on} = I_L + \frac{1-d}{d} I_{L1} = \frac{I_L}{d} \quad (28)$$

$$i_{c1-on} = \frac{1-d}{d} I_{L1} \quad (29)$$

In addition to the average input, the current expression is given by,

$$I_{in} = d i_{in-on} + (1-d) i_{in-off} = I_L + (1-d) i_L = (2-d) I_L \quad (30)$$

Taking $T = 1/f$ into consideration,

$$\frac{V_{in}}{I_{in}} = \left(\frac{1-d}{2-d}\right)^2 \frac{V_0}{I_0} = \left(\frac{1-d}{2-d}\right)^2 R \quad (31)$$

The inductor current i_L fluctuation ratio is,

$$\xi_1 = \frac{\Delta i_L/2}{I_L} = \frac{d(2-d)TV_{in}}{2L_I I_{in}} = \frac{d(1-d)^2}{2(2-d)fL} \quad (32)$$

When output voltage V_o is rippled, it is

$$\Delta V_o = \frac{\Delta Q}{C_2} = \frac{I_0(1-d)T}{C_2} = \frac{1-d}{fC_2}\frac{V_0}{R} \quad (33)$$

Consequently, the output voltage's variation ratio, V_o is

$$\varepsilon = \frac{\Delta V_0/2}{V_0} = \frac{1-d}{2fRC_2} \quad (34)$$

The T2 FLC-based MPPT technique is used to derive the optimum energy possible from solar panels. Additionally, it has other advantages, including reducing fluctuations and providing an instantaneous response to changes in solar irradiation (shading effect). The following section discusses the proposed MPPT approach in more depth.

3.4. Modelling of Type-2 Fuzzy-Based MPPT Controller

The FLC, which has many applications specifically in control theory using FLC reduces the demand for a reliable mathematical model of a system, and it is also non-linear, adaptable, and robust to both parametric and non-parametric variation. FLC transform linguistic control inputs into numerical control data by simulating human cognitive processes for control actions. The decision-making capacity of a fuzzy controller allows it to incorporate expert information. Fuzzification, inference, and defuzzification are the three components of fuzzy logic.

Using a proper transformation function, the fuzzification converts an uncertain parametric value into a set of fuzzified values. Triangular fuzzy functions have been evaluated in the current work. These functions have any number, but the more functions that are taken into consideration, the better the accuracy is obtained. However, this is going to increase processing time and memory constraints, whereas the accuracy level decreases with a lower number of functions. Five membership functions that have good accuracy without complicating the system have been chosen to address these shortcomings.

Moreover, the fuzzy membership set of values is a defined collection of values. To solve the real problems, including partial shading application, the T2 FLC is employed. Because the values of fuzzy in these situations typically fall within the footprint of the uncertainty band rather than being sharp. The centre of the membership function is more sensitive for the T2 FLC. It provides greater flexibility in data uncertainties, including unclear weather conditions, and it overcomes the drawbacks of type-1 FLC. The representation of T2 FLC is shown in Figure 6. The fuzzifier is given the PV array's sensing outputs. The inference engine uses the output processing block to further defuzzify the output from the fuzzifier based on the knowledge base.

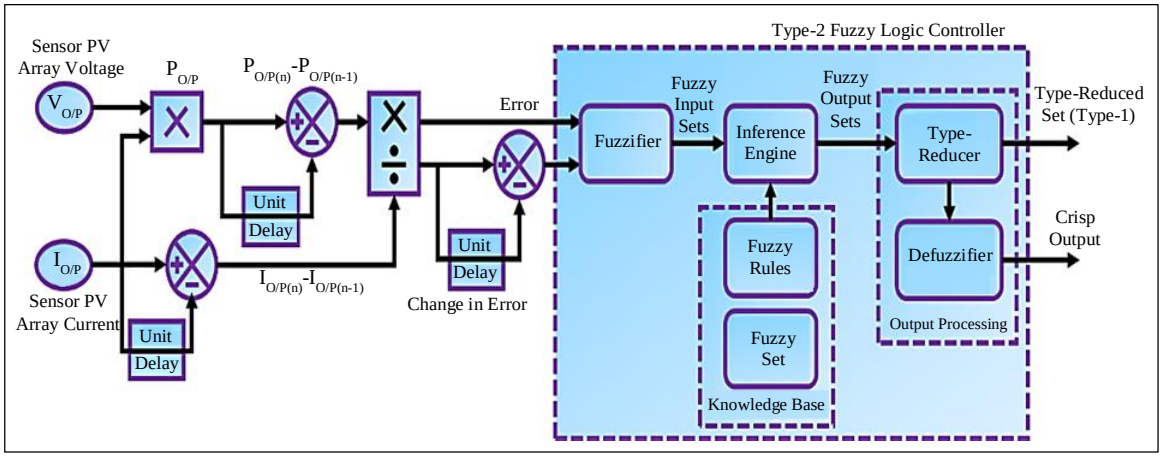

Fig. 6 Proposed fuzzy logic controller (Type-2)

The main elements (rule base, fuzzy logic, and interface machine and output processing unit) of the T2 FLC structure are identical compared to its T1 FLC analogues. Meanwhile, the output processor for a T2 FLC is comprised of type reduction to an IT1 FLC and defuzzification. The type reduction methods and fuzzy operators of a T2 FLC's inference machine correspond to the T1 FLC, with the exception that a T2 FLC has T2 FLCs for its inputs and outputs.

D Error / Error	-B	-S	Z_0	+S	+B
-B	Z_0	Z_0	+B	+B	+B
-S	Z_0	Z_0	+S	+S	+S
$-Z_0$	+S	Z_0	Z_0	Z_0	-S
+S	-S	-S	-S	Z_0	Z_0
+B	-B	-B	-B	Z_0	Z_0

Fig. 7 Fuzzy rule with two input variable (error and change in error)

The rule base matrix is displayed in Figure 7. Depending on the active state of the input membership function, control action is modified. For inferencing, Mamdani's MAX-MIN approach is utilized in this work. Each rule output membership is given by the minimum operator. Meanwhile, the maximal operator produces combined fuzzy results.

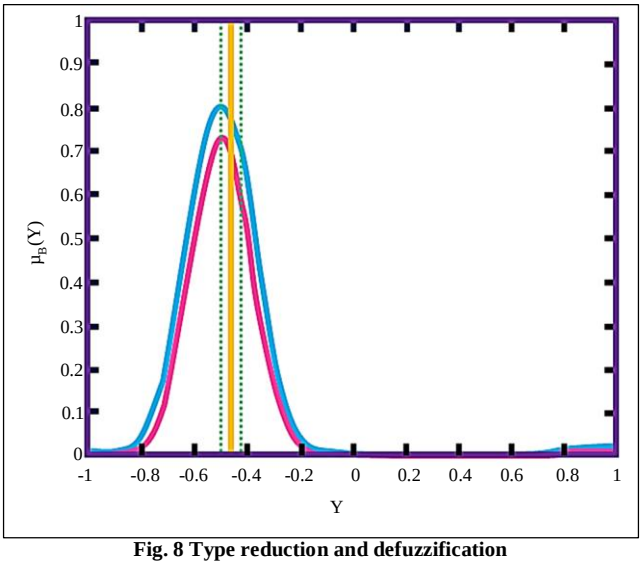

Fig. 8 Type reduction and defuzzification

Figure 8 displays the defuzzification and type-reduction. Using the Matlab computer program, the type-2 with accompanying operations is implemented to obtain certain outcomes. Thus, the proposed T2 FLC-based MPPT algorithm extracts the most power from the PV panel and enhances the converter performance.

3.5. Reference Current Generation Using Pi Controller Assisted D-Q Theory Method

The $dq0$ transformation is utilized for converting the reference current produced from the load current, which includes the harmonic elements i_{La}, i_{Lb} and i_{Lc} to give i_d, $\mathrm{i_q}$ and $\mathrm{i_o}$. The DQ transformation is used to govern the grid-coupled circuit.

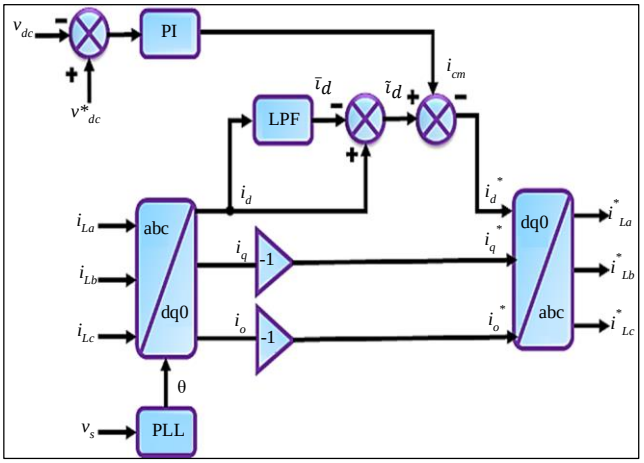

Fig. 9 Reference current generation by DQ theory

The id is then reliably sent via an LPF filter, as shown in Figure 9, the structure in order to optimize the efficiency of the process and output production speed.

When the dynamic DC element is subtracted from the $\widetilde{\imath d}$ on the d axis, an AC component with a harmonic value and no fundamental ti_d is produced. Furthermore, to maintain the transient state and magnitude of the reference current and approach, the inverter DC voltage regulator, a power supply connected to an inverter circuit with PI regulation, is used to create $\widetilde{\imath d}$, which is later modified by i_{cm} .

However, for null axis and quadrature currents, the magnitude is reversed. Additionally, the $dq0$ axis function performed a second transformation that produced the amount abc and the elements $i*_{La}$, $i*_{Lb}$ and $i*_{Lc}$. The suggested PI-based control solution also successfully synchronizes the grid while achieving reduced harmonic contents.

3.6. Shunt Compensator Control

In a PV-UPQC system, a shunt compensator performs multiple functions, including the maintenance of DC link voltage, compensation of reactive power demand, mitigation of harmonics, and extraction of maximum power from the solar PV array.

It injects voltage which is either in phase or out of phase with the PCC voltage. The compensation of load current is achieved by extracting its active fundamental component. This is accomplished by using the DQ theory to operate the shunt converter, as seen in Figure 10.

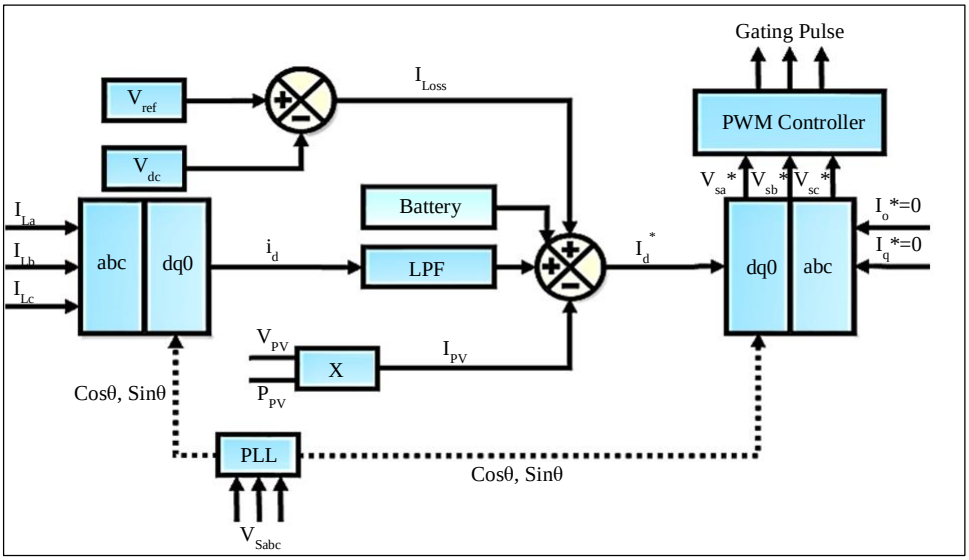

Fig. 10 Shunt compensator control

3.7. Series Compensator Control

In a PV-UPQC system, the series compensator stabilizes the load voltage by injecting a voltage with the same frequency and phase as the load voltage. It also injects a voltage with the inverse phase when voltage sags or swells occur. The series compensator also removes distortions in the voltage waveform caused by harmonics and sags or swells. Figure 11 provides the structure of control of the series compensator of UPQC.

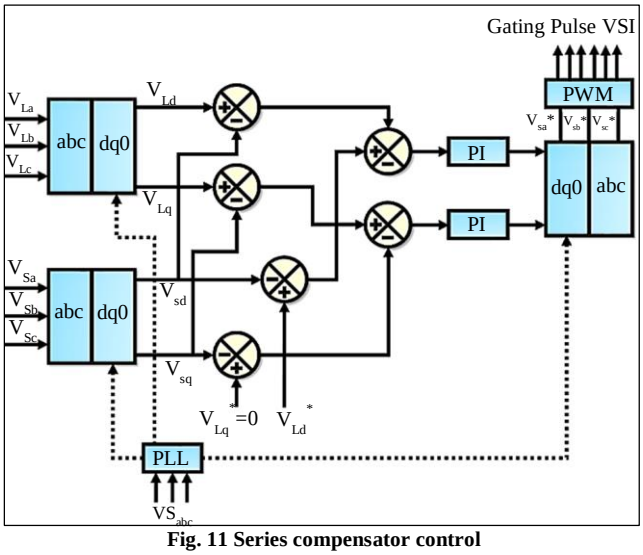

Fig. 11 Series compensator control

4. Results and Discussion

This article uses control strategies for each part to expand on the PQ enhancement. The proposed method is more effective in resolving PQ problems such as voltage swell and sag. MATLAB platform is used to verify the performance of the proposed system. Table 1 outlines the parameter specifications of the proposed system.

Table 1. System parameter specification

Parameter	Specification
Photovoltaic System	
Short Circuit Current	$8.33A$
Open Circuit Voltage	$12V$
Peak Power	$10KW$, 10 Panels
Series connected solar PV cells	36
Super Lift Luo converter	
Inductor L	3.6 mH
Capacitor C_1	4.7 mH
Capacitor C_2	2200 μ

The solar panel parameters, including voltage, current, temperature and irradiation, are represented in Figure 12. The observation indicates stability in both temperature and irradiation with values of 35°C and 1000 $W/Sq.m$. Similarly, the solar panel's constant voltage and current attained the value of 70V and 175 Amps, respectively. The obtained voltage and current of the PV panel are further improved with the help of the proposed converter.

Figure 13 demonstrates the proposed converter output current and voltage. A stabilized voltage of 100V is attained, and the current requires 0.1 seconds to maintain a constant value of 10 Amps. The findings are examined for voltage sag and swell situations, and the remaining two cases are discussed in detail.

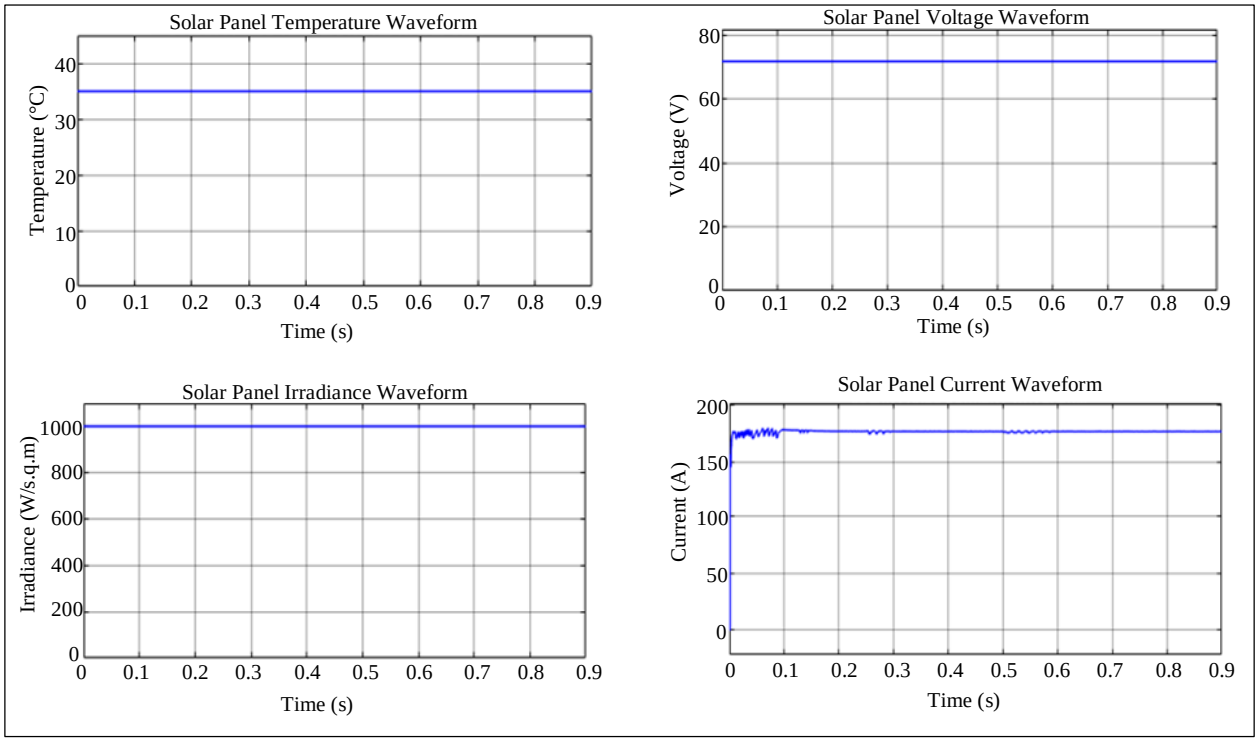

Fig. 12 Waveforms indication of PV panel parameters

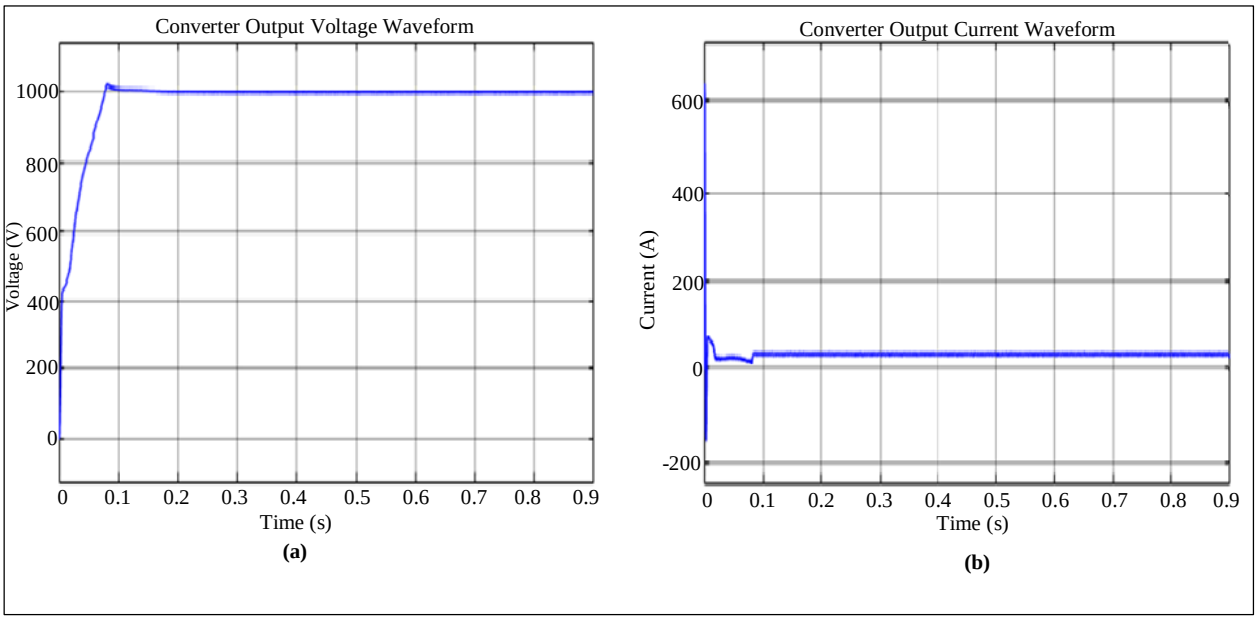

Fig. 13 Waveforms indication of super lift luo converter output (a) Voltage, and (b) Current.

4.1. Case 1: Step Magnitude (-0.3)

The voltage sag is examined in this part; the sag occurs at 0.4s to 0.6s, as shown in Figure 14; the voltage is originally at 400V, and if there is a sag, it is indicated that the voltage is dropped; at this point, the current appears to be raised to 55Amps. The equivalent source current and voltage are also indicated, with a decrease in voltage and a rise in current. Figure 15 also includes the improved power factor waveform. The source voltage and current depiction display PQ difficulties; thus, the system is evaluated when the control methods are applied. The T2 FLC method is used to regulate the converter output, while the PI controller is used for managing the UPQC. Although the source parameters vary in voltage, the load current and voltage do not, as seen in Figure 15. The problem of voltage sag is not apparent in load current and voltage representations from 0.1s to 0.2s.

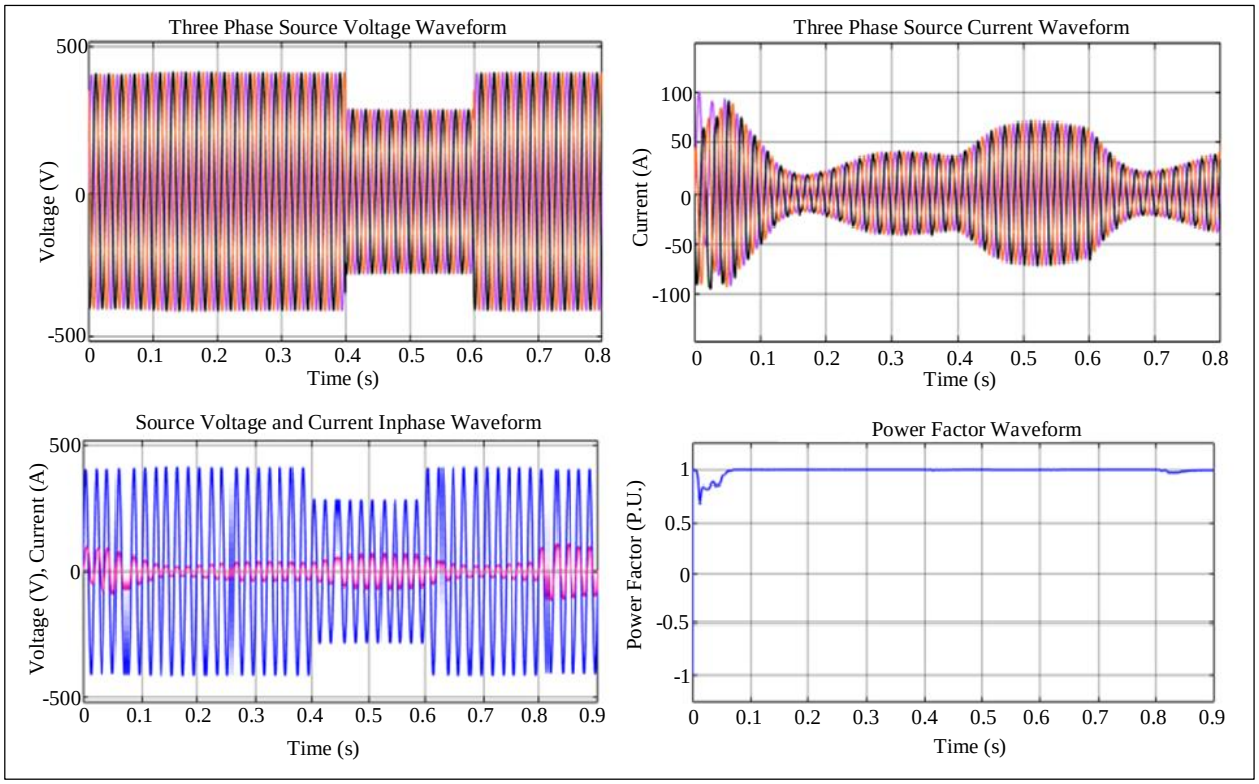

Fig. 14 Voltage sag analysis

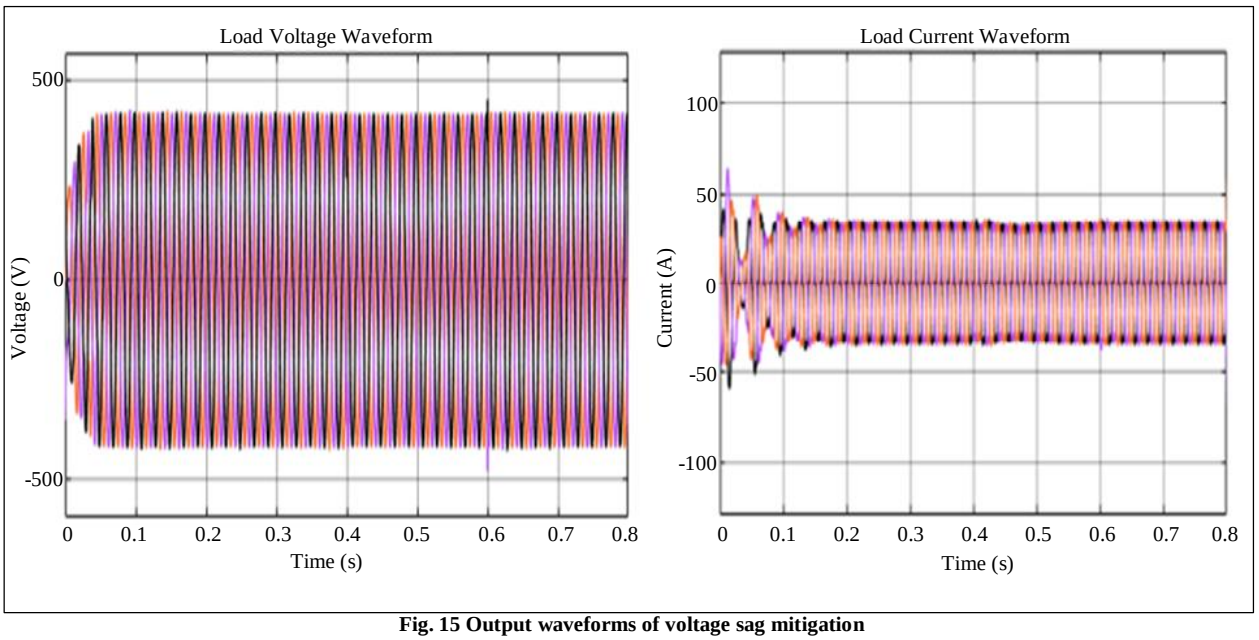

Fig. 15 Output waveforms of voltage sag mitigation

Case 2: Step Magnitude (+0.3)

The voltage swell continues to be examined in this part in the same way as it occurred in case (I); from 0.4s to 0.6s, there is a voltage swell, and at that point, the voltage achieves 550V, and at the remaining time, the voltage is at 400V, as shown in Figure 16, that is also represented in the current waveform. According to the figure, the source current and voltage are in phase and have a unity power factor. Despite the fact that there is a voltage swell on the source side, Figure 17 shows that the voltage swell is reduced with the help of the control method. The load voltage is still 400V, and the load current is approximately 40 Amps. The system accomplishes reduced THD of 2.02%, which is the lowest THD value when compared to another conventional method.

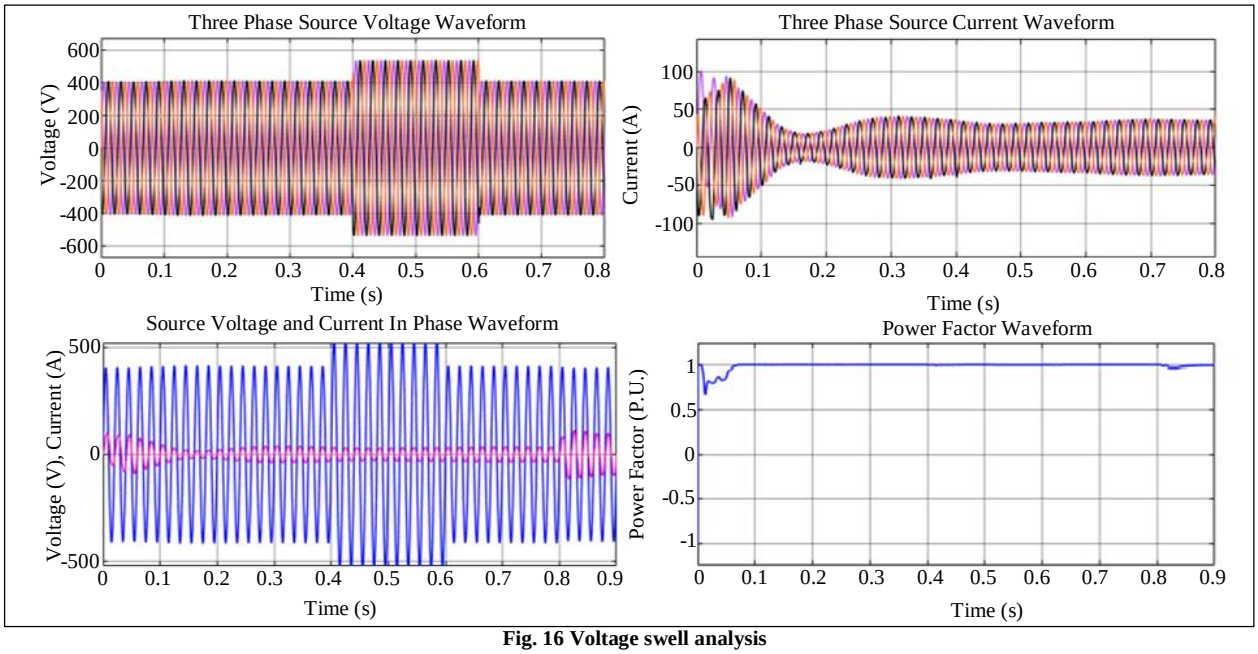

Fig. 16 Voltage swell analysis

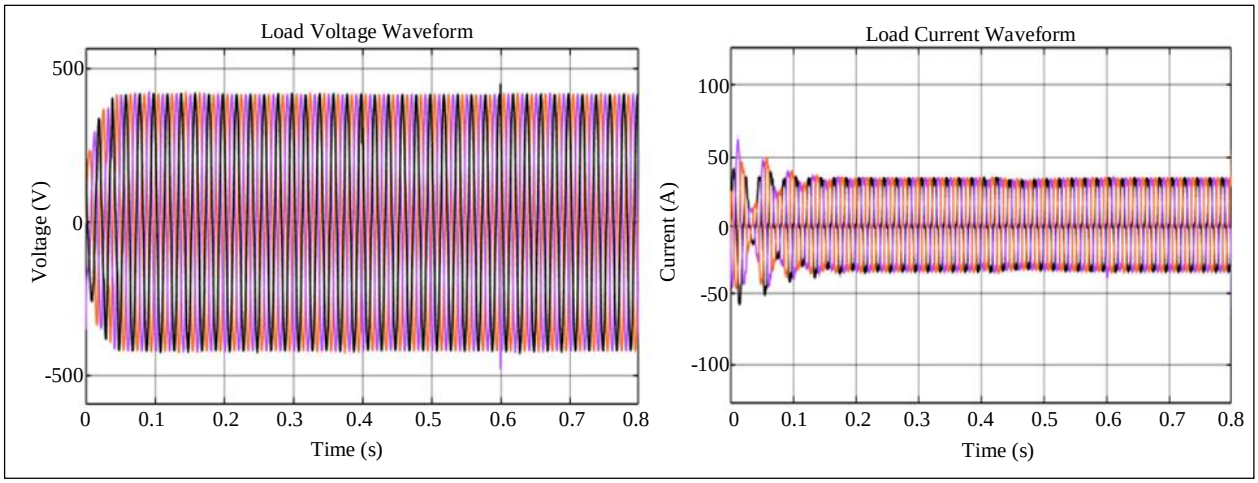

Fig. 17 Output waveforms of voltage swell mitigation

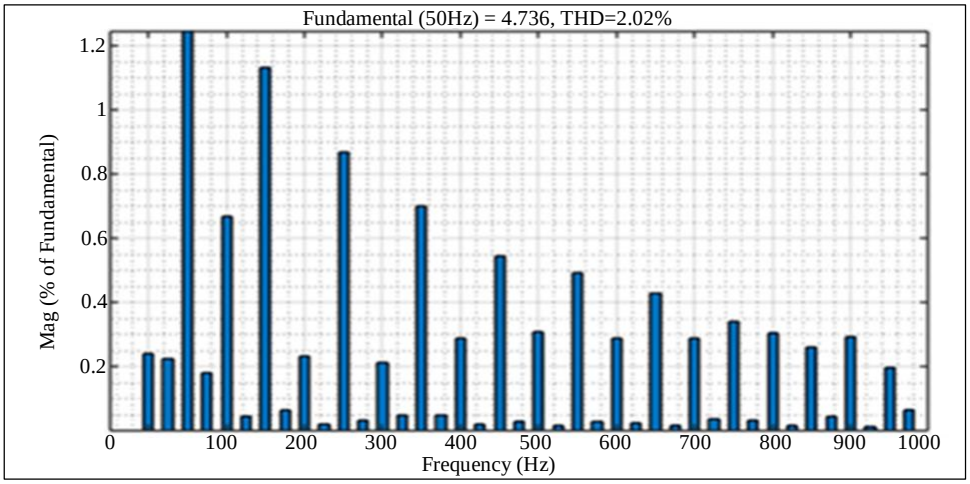

Fig. 18 THD waveform

Table 2. Comparative study of efficiency analysis

Converter Types	Efficiency (%)
Boost	80 [25]
Cuk	85 [26]
SEPIC	88.82 [27]
Luo	90 [28]
Super Lift Luo	96.4

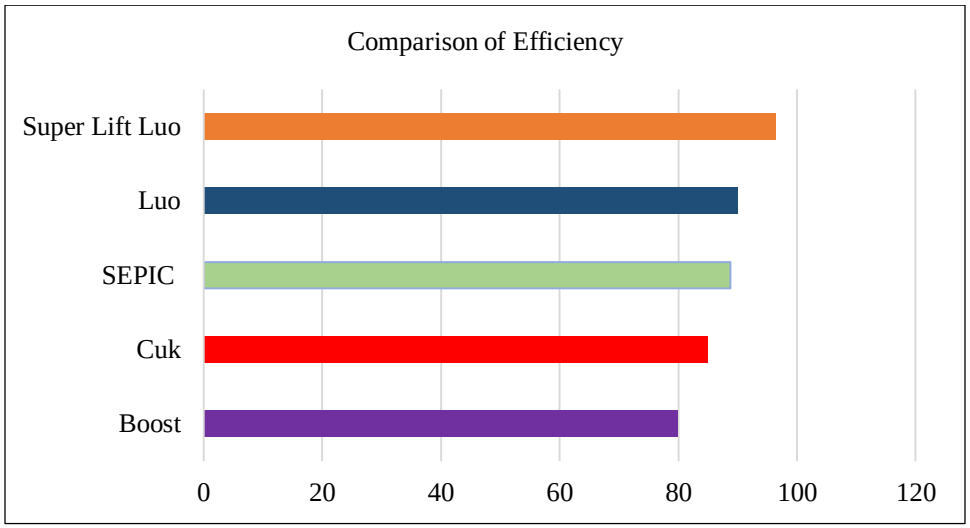

Fig. 19 Comparison of efficiency

Based on Table 2, it is evident that the proposed Super lift Luo converter outperforms in terms of efficiency in contrast to other existing converters, including Boost, Cuk, SEPIC, and Luo converters. The proposed converter attains an improved efficiency value of 96.4%, as shown in Figure 19. Table 3 represents the comparison evaluation of various converter components with the proposed converter. According to Table 4, the proposed UPQC system achieves power factor unity under both sag and swell scenarios as contrasted without the UPQC system.

Table 3. Comparison with other converters

Parameters	Boost [25]	Cuk [26]	SEPIC [27]	Luo [28]	Super Lift Luo converter
No. of Switches	1	1	1	1	1
No. of Diodes	1	1	1	2	2
No. of Capacitors	1	2	3	2	2
No. of Inductors	1	2	2	1	2
Total Number of Components	4	6	7	6	6

Table 4. Effectiveness of the UPQC strategy in terms of power factor

Circuits	Power Factor	
	Sag	Swell
With no UPQC	0.69	0.71
With UPQC	0.967	0.977

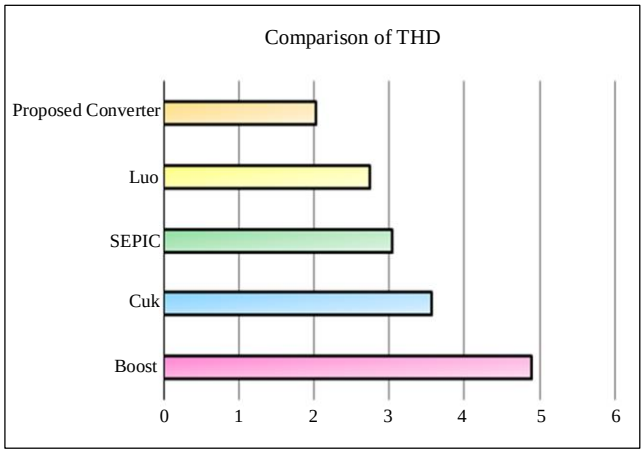

Fig. 20 THD Comparison

Figure 20 depicts the THD comparison among the proposed converter and various current converters. This explains that the proposed Super Lift Luo converter has a THD value of approximately 2.02%, which is considerably less than that of the other converters.

Table 5. Comparison of UPQC control

Reference	Source Current THD %			Dynamic Response
	A	B	C	
[22]	2.18%	2.24%	2.26%	Medium
[23]	2.96%	2.95%	2.96%	Low
[24]	2.5%	2.59%	2.41%	Low
Proposed	2.02%	1.98%	2.04%	Fast

The proposed UPQC control technique, when compared with several other techniques, has low source current THD and quick dynamic response, as seen in Table 5.

The proposed control for UPQC improves PQ by effectively alleviating any irregularities in voltage. The optimal control of DC bus voltage and the dynamic adjustment of UPQC control signals improve the stability of the entire system. The stable load side voltage and current waveforms are credited to the exceptional compensation ability of the proposed work. Moreover, it also achieves a near unity power factor. The implementation of the Super-Lift Luo converter also has a crucial role in enhancing the output of the proposed work. These qualities allow the proposed approach to achieve better results than existing techniques.

5. Conclusion

In conclusion, the integration of a Super-Lift Luo converter with a solar energy system and a Battery Integrated UPQC offers a promising solution for enhancing power quality and facilitating the incorporation of renewable energy sources in microgrid systems. The MPPT control structure using T2 FLCs enables the adjustment of the output voltage and ensures a reliable power supply to loads. The battery is employed to store the energy generated by the PV panel.

The saved energy is utilized when solar power production is low, or the demand for load is extreme. In addition, utilizing PI controller-assisted DQ theory, current harmonics are removed. The results accomplished demonstrate that the proposed system achieves a remarkable efficiency of 96.4% while effectively reducing the THD to a minimal value of 2.02%.

References

[1] Leonardo Bruno Garcia Campanhol et al., "Single-Stage Three-Phase Grid-Tied PV System With Universal Filtering Capability Applied to DG Systems and AC Microgrids," *IEEE Transactions on Power Electronics*, vol. 32, no. 12, pp. 9131-9142, 2017. [CrossRef] [Google Scholar] [Publisher Link]

[2] Pragnyashree Ray, Pravat Kumar Ray, and Santanu Kumar Dash, "Power Quality Enhancement and Power Flow Analysis of a PV Integrated UPQC System in a Distribution Network," *IEEE Transactions on Industry Applications*, vol. 58, no. 1, pp. 201-211, 2021. [CrossRef] [Google Scholar] [Publisher Link]

[3] Santanu Kumar Dash, and Pravat Kumar Ray, "Power Quality Improvement Utilizing PV Fed Unified Power Quality Conditioner Based on UV-PI and PR-R Controller," *CPSS Transactions on Power Electronics and Applications*, vol. 3, no. 3, pp. 243-253, 2018. [CrossRef] [Google Scholar] [Publisher Link]

[4] Hina Mahar et al., "Implementation of ANN Controller Based UPQC Integrated with Microgrid," *Mathematics*, vol. 10, no. 12, pp. 1-24, 2022. [CrossRef] [Google Scholar] [Publisher Link]

[5] Leonardo Bruno Garcia Campanhol et al., "Power Flow and Stability Analyses of a Multifunctional Distributed Generation System Integrating a Photovoltaic System With Unified Power Quality Conditioner," *IEEE Transactions on Power Electronics*, vol. 34, no. 7, pp. 6241-6256, 2019. [CrossRef] [Google Scholar] [Publisher Link]

[6] Varadharajan Balaji, and Subramanian Chitra, "Power Quality Management in Electrical Grid Using SCANN Controller-Based UPQC," *Bulletin of the Polish Academy of Sciences, Technical Sciences*, vol. 70, no. 1, pp. 1-9, 2022. [CrossRef] [Google Scholar] [Publisher Link]

[7] Koganti Srilakshmi et al., "Artificial Intelligence based Multi-Objective Hybrid Controller for PV-Battery Unified Power Quality Conditioner," *International Journal of Renewable Energy Research*, vol. 12, no. 1, pp. 495-504, 2022. [CrossRef] [Google Scholar] [Publisher Link]

[8] Javed Ahmad et al., "A New High-Gain DC-DC Converter with Continuous Input Current for DC Microgrid Applications," *Energies*, vol. 14, no. 9, pp. 1-14, 2021. [CrossRef] [Google Scholar] [Publisher Link]

[9] Yonghao Gui et al., "Large-Signal Stability Improvement of DC-DC Converters in DC Microgrid," *IEEE Transactions on Energy Conversion*, vol. 36, no. 3, pp. 2534-2544, 2021. [CrossRef] [Google Scholar] [Publisher Link]

[10] Pandav Kiran Maroti et al., "New Tri-Switching State Non-Isolated High Gain DC–DC Boost Converter for Microgrid Application," *IET Power Electronics*, vol. 12, no. 11, pp. 2741-2750, 2019. [CrossRef] [Google Scholar] [Publisher Link]

[11] Xiangke Li et al., "A Novel Assorted Nonlinear Stabilizer for DC–DC Multilevel Boost Converter with Constant Power Load in DC Microgrid," *IEEE Transactions on Power Electronics*, vol. 35, no. 10, pp. 11181-11192, 2020. [CrossRef] [Google Scholar] [Publisher Link]

[12] Ali M. Jasim, Basil H. Jasim, and Bogdan-Constantin Neagu, "A New Decentralized PQ Control for Parallel Inverters in Grid-Tied Microgrids Propelled by SMC-Based Buck-Boost Converters," *Electronics*, vol. 11, no. 23, pp. 1-24, 2022. [CrossRef] [Google Scholar] [Publisher Link]

[13] K. Vasudevan, and R. Ramesh, "Power Quality Analysis of Hybrid Cuk Converter Based on Micro Grid Distributed Power Generation System," *Journal of Electrical Engineering*, vol. 18, no. 4, 2018. [Google Scholar]

[14] Harish Chandra Mohanta et al., "An Optimized PI Controller-Based SEPIC Converter for Microgrid-Interactive Hybrid Renewable Power Sources," *Wireless Communications and Mobile Computing*, vol. 2022, no. 1, pp. 1-10, 2022. [CrossRef] [Google Scholar] [Publisher Link]

[15] P. Sivagami, and N.M. Jothiswaroopan, "Optimal Control Strategy Using PV Based LUO Converter for a Micro Grid to an Unelectrified Zone," *Journal of Green Engineering*, vol. 10, pp. 463-479. [Google Scholar]

[16] Hemanth Kumar Raju Alluri et al., "Optimal Tuning of PI Controllers for DFIG-Based Wind Energy System Using Self-adaptive Differential Evolution Algorithm," *International Journal on Electrical Engineering and Informatics*, vol. 11, no. 2, pp. 352-372, 2019. [CrossRef] [Google Scholar] [Publisher Link]

[17] Meenakshi Rastogi, Aijaz Ahmad, and Abdul Hamid Bhat, "Performance Investigation of Two-Level Reduced-Switch D-STATCOM in Grid-Tied Solar-PV Array with Stepped P&O MPPT Algorithm and Modified SRF Strategy," *Journal of King Saud University-Engineering Sciences*, vol. 35, no. 6, pp. 393-405, 2021. [CrossRef] [Google Scholar] [Publisher Link]

[18] Oumnia Lagdani, Mourad Trihi, and Badre Bossoufi, "PV Array Connected to the Grid with the Implementation of MPPT Algorithms (INC, P&O and FL Method)," *International Journal of Power Electronics and Drive Systems*, vol. 10. 4, pp. 2084-2095, 2019. [CrossRef] [Google Scholar] [Publisher Link]

[19] Vinit Kumar, and Mukesh Singh, "Derated Mode of Power Generation in PV System Using Modified Perturb and Observe MPPT Algorithm," *Journal of Modern Power Systems and Clean Energy*, vol. 9, no. 5, pp. 1183-1192, 2020. [CrossRef] [Google Scholar] [Publisher Link]

[20] Lijun Zhao et al., "Grid-Tied PV-BES System Based on Modified Bat Algorithm-FLC MPPT Technique under Uniform Conditions," *Neural Computing and Applications*, vol. 33, pp. 14929-14943, 2021. [CrossRef] [Google Scholar] [Publisher Link]

[21] Damodhar Reddy, and Sudha Ramasamy, "A Fuzzy Logic MPPT Controller Based Three Phase Grid-Tied Solar PV System with Improved CPI Voltage," *2017 Innovations in Power and Advanced Computing Technologies (i-PACT)*, Vellore, India, pp. 1-6, 2017. [CrossRef] [Google Scholar] [Publisher Link]

[22] Tao Jin et al., "An Effective Compensation Control Strategy for Power Quality Enhancement of Unified Power Quality Conditioner," *Energy Reports*, vol. 6, pp. 2167-2179, 2020. [CrossRef] [Google Scholar] [Publisher Link]

[23] Hina Mahar et al., "Implementation of ANN Controller Based UPQC Integrated with Microgrid," *Mathematics*, vol. 10, no. 12, 2022. [CrossRef] [Google Scholar] [Publisher Link]

[24] Tongfei Lei et al., "Performance Analysis of Grid-Connected Distributed Generation System Integrating a Hybrid Wind-PV Farm Using UPQC," *Complexity*, 2022. [CrossRef] [Google Scholar] [Publisher Link]

[25] Farzam Nejabatkhah et al., "Modeling and Control of a New Three-Input DC–DC Boost Converter for Hybrid PV/FC/Battery Power System," *IEEE Transactions on Power Electronics*, vol. 27, no. 5, pp. 2309-2324, 2011. [CrossRef] [Google Scholar] [Publisher Link]

[26] Francarl Galea et al., "Design of a High Efficiency Wide Input Range Isolated Cuk Dc-Dc Converter for Grid Connected Regenerative Active Loads," *World Federation of Engineering Organizations*, pp. 1-11, 2011. [Google Scholar] [Publisher Link]

[27] Patan Javeed et al., "SEPIC Converter for Low Power LED Applications," *Iraqi Academics Syndicate International Conference for Pure and Applied Sciences*, Babylon, Iraq, vol. 1818, pp. 1-19, 2020. [CrossRef] [Google Scholar] [Publisher Link]

[28] S. Sivarajeswari, and D. Kirubakaran, "Retracted: Design and Development of Efficient Luo Converters for DC Micro Grid," *International Journal of Electrical Engineering & Education*, vol. 60, no. 1, pp. 40-48, 2023. [CrossRef] [Google Scholar] [Publisher Link]